IOP Publishing
Journal of Micromechanics and Microengineering
J. Micromech. Microeng. **32** (2022) 044003 (8pp)
https://doi.org/10.1088/1361-6439/ac542b

A triboelectric nanosensor based on ultra-thin MXene composite paper for heavy metal ion detection

Engui Wang[1,2,3], Yu Cao[3], Yuan Bai[2,3], Yansong Gai[3], Yizhu Shan[3,4], Qi Li[3], Tao Jiang[1,2,3,4], Hongqing Feng[3,4,*] and Zhou Li[2,3,4,*]

[1] School of Resources, Environments and Materials, Guangxi University, Nanning 530004, People's Republic of China
[2] Center of Nanoenergy Research School of Physical Science and Technology, Guangxi University, Nanning 530004, People's Republic of China
[3] Beijing Institute of Nanoenergy and Nanosystems, Chinese Academy of Sciences, Beijing 101400, People's Republic of China
[4] School of Nanoscience and Technology, University of Chinese Academy of Sciences, Beijing 100049, People's Republic of China

E-mail: fenghongqing@binn.cas.cn and zli@binn.cas.cn

Received 20 December 2021, revised 23 January 2022
Accepted for publication 9 February 2022
Published 24 February 2022

Abstract

Heavy metal pollution has become increasingly serious in recent decades with the progress of industrialization, posing a significant threat to human health. This raises the demand for portable and ease of use heavy metal ion detection devices. In this study, we develop ultra-thin (5 μm) and highly flexible composite paper of MXene/bacterial cellulose (M/BC$_x$, with x denoting the BC content) and apply it in a self-powered triboelectric nanosensor (TENS) to do heavy metal ion detection. The M/BC$_x$ composite paper is fabricated using a simple vacuum filtration method, and combines the advantages of the high electrical conductivity of MXene with the excellent mechanical properties of BC. The TENS employs the M/BC$_x$ composite paper and polytetrafluoroethylene as the friction layers, and the influences of different ratios of M/BC$_x$ on the electrical signals is investigated. The TENS shows high sensitivity in the detection of Cu^{2+}, Cr^{3+}, and Zn^{2+}, as the detection limit is as low as 1 μM without the need of ligand molecules. A linear range of 10–300 μM is obtained. The TENS also shows excellent stability after more than 10 000 continuous operations. This simple-structured, cost-effective and durable TENS device provides new insights into the methodology of heavy metal ion detection and can be further developed for the detection of the corresponding ions in serum.

Supplementary material for this article is available online

Keywords: triboelectric nanosensor, MXene, bacterial cellulose, heavy metal ion detection, self-power

(Some figures may appear in colour only in the online journal)

* Authors to whom any correspondence should be addressed.

1. Introduction

With the development of industrialization, heavy metal pollution has become more and more serious [1–4]. Excess heavy metals can accumulate biologically and eventually pass along the food chain to the human body. Most heavy metals are toxic or carcinogenic and eventually pose a serious threat to human health [5]. Increasing attention has been paid to the detection and removal of heavy metal ions [6–8]. However, most of these techniques require sophisticated and expensive equipment, professional operators, and external power sources, which greatly limits the application of these techniques [9].

In 2012, Zhonglin Wang's team invented triboelectric nanogenerators (TENGs) [10]. Based on the coupling of triboelectric effect and electrostatic induction, TENG can convert mechanical energy into electric output [11–14]. With the intensive study of TENG, the concept of triboelectric nanosensor (TENS) has also been developed [15–19]. The self-powered sensing is achieved by influencing the TENS output with the electric charges carried by the detected object. Wang *et al* prepared a self-powered TENS for the detection of dopamine under alkaline conditions [20]. Li *et al* proposed to load ligand molecules on the surface of the friction layer of a TENS to detect heavy metal ions with a detection range of 40–200 μM [21]. Another group developed a TENS for catechin detection, and high sensitivity (detection limit of 5 μM) was achieved due to the strong interaction of Ti atoms in the nano-TiO_2 material with the catechin enediol group [22]. Wang *et al* demonstrated a TENS for Hg^{2+} ion detection using 3-mercaptopropionic acid (3-MPA)-modified Au NPs as electrical enhancers and recognition elements [23]. The advantage of TENS for ion detection is that it is self-powered and does not require complex instrumentation, but the sensitivity of TENS detection is low [24].

2D materials are considered to be powerful materials for sensing platforms due to their large specific surface area, dense surface active sites, easy interfacial transport and short diffusion paths [25, 26]. Combining fluorescence, surface-enhanced Raman scattering, surface plasmon resonance, field-effect transistors, and electrochemistry, 2D material-based sensing platforms have been used to detect heavy metal ions, organic compounds, pesticide residues, antibiotics, nucleic acids, proteins, bacteria, and cells. However, all of these 2D material sensing platforms rely on expensive and sophisticated instruments as well as external power sources, making *in situ* detection impossible [27–29]. MXene is a graphene-like 2D material composed of transition metal carbides/nitrides and carbonitrides [24]. Pure MXene has great application limitations due to its poor mechanical properties. To solve this problem, polymers and metal nanowires have been used as reinforcing agents for MXene, but their high cost greatly limits the future commercial application [30]. Bacterial cellulose (BC) nanofibers are organic compounds that are low-cost, abundantly available, easy to prepare, and environmentally friendly. BC nanofibers have been used together with MXene in wound repair [31], supercapacitors [32], carbon aerogel [33], electromagnetic interference shielding [34]. However, the application of MXene/BC on TENS for material sensing has never been reported.

In this study, we develop a MXene/BC based TENS to do heavy metal ion detection, addressing the problems of high cost, complicated operation process and sophisticated device requirement of present metal ion detection methods. Ultra-thin composite paper based on MXene/BC (M/BC$_x$, with x indicating BC content) is successfully fabricated and used for the detection of heavy metal ions in TENS. The large number of radicals on the surface of 2D MXene nanosheets act as active sites that bind to heavy metal ions and alter the ability of M/BC$_x$ to gain and lose electrons in the TENS, enabling a high sensitivity for heavy metal ion detection. The M/BC$_x$ TENS functions well in the detection of Cu^{2+}, Cr^{3+}, and Zn^{2+} in a range of 1–300 μM (the concentration range specified by WHO [35]), under the condition that no ligand molecules are used. This TENS also has excellent stability after more than 10 000 consecutive operations. The TENS based on the ultra-thin M/BC$_x$ composite paper has good potential in the fields of heavy metal ion detection in water environment, as well as for the detection of the corresponding ions in serum.

2. Materials and methods

2.1. Preparation of MXene materials

(a) Etching: take 30 ml of 36%–38% hydrochloric acid, and add 10 ml of deionized water to dilute it; add 2 g of lithium fluoride, put in magnetic mixers to stir the mixed solution, add 2 g of MAX phase (Ti_3AlC_2) and stir the mixture at 40 °C for 24 h;
(b) De-acidification after etching: divide 40 ml of the above mixture into two centrifuge tubes, add deionized water to 35 ml and centrifuge (3500 rpm, 3 min); then discard the supernatant, rinse with 35 ml deionized water and centrifuge again. Repeat this step until the pH of the supernatant drops to 6.0;
(c) Sonication after de-acidification: add deionized water to 35 ml and do sonication in an ice bath for 1 h [36].

2.2. Preparation of M/BC$_x$ composite paper

Figure 1 illustrates the process of preparing M/BC$_x$ composite paper by vacuum filtration. BC fibers are purchased from Guilin Qihong Technology Co., Ltd, China. The fibers have a diameter range of 50–100 nm and a length of about 20 μm. Firstly, Ti_3AlC_2 is etched by a mixture of lithium fluoride and hydrochloric acid; then 10 mg ml^{-1} of MXene solution is obtained by ultrasonic delamination. Take 0.5 ml of MXene solution with a concentration of 10 mg ml^{-1} and 0.625 g of BC with a mass fraction of 0.8% and dilute to 10 ml, to make M/BC$_{0.5.}$ The mixed solution of M/BC$_{0.5}$ is obtained after sonication in ice bath, and the M/BC$_{0.5}$ composite paper is formed by vacuum filtration. In similar way, M/BC$_x$ is obtained by changing the mass ratio of MXene and BC.

Figure 1. Fabrication process of the M/BC$_x$ composite paper.

2.3. M/BC$_x$-TENG fabrication

The Cu tape is adhered to the surface of polytetrafluoroethylene (PTFE) and cut into a circle with a diameter of 36 mm. Cu/PTFE is pasted to a polymethyl methacrylate (PMMA) plate as one contact layer and electrode. On another PMMA plate, the M/BC$_x$ composite paper is pasted, and serves as the other contact layer and electrode. The two plates are connected by four springs mounted at their corners, and the distance between the M/BC$_x$ paper and PTFE is 20 mm.

2.4. Characterization and measurement

Microscopic morphological observations of the M/BC$_x$ composite paper are performed using a field emission SEM (NOVA450, Czech Republic) at an accelerating voltage of 10 kV. Crystal and elementary composition are analyzed by x-ray diffractometer (XRD, PANalytical X′Pert) with Cu Kα radiation ($\lambda = 1.5406$ Å, $2\theta = 5°$–$40°$, step size of 0.01). A linear motor (LinMot E1100) is applied to provide periodic contact-separation movement for the M/BC$_x$-TENG electrical measurements. The V_{OC}, I_{SC}, and Q_{SC} of the M/BC$_x$-TENG are measured by a Keithley 6517 electrometer and recorded by an oscilloscope (LeCroy HDO6104).

2.5. Heavy metal ion detection

To evaluate the sensitivity of TENS for the detection of metal ions, a mechanical linear motor (LinMot E1100) is used to provide periodic contact separation motion. The maximum moving distance is 20 mm and the operating frequency is 1 Hz. Constant volumes of heavy metal ion solutions (20 μl) are dropped onto the surface of M/BC$_{0.5}$ composite paper. After drying at ambient temperature (24 °C), electrical measurements are performed.

3. Results and discussion

3.1. Characterization of the M/BC$_x$ composite paper

The morphology and microstructure of the M/BC$_x$ composite paper are observed using SEM. Figure 2 shows the microscopic morphology of the composite paper with different BC contents, in which it can be observed that a large number of 1D BC fibers are randomly distributed and 2D MXene nanosheets are loaded on them. As the BC content increases, more fibrous structures appear on the surface for the connection between MXene. With the increase of BC content, the fibers become more and more dense. The cross-sectional electron micrographs show that the thickness of the composite paper increases with increasing BC content, and the thickness of the M/BC$_{0.5}$ composite paper is 4.724 μm (figures 2(c) and 3). These results suggest that this composite structure greatly improves the mechanical strength of the composite paper. Figure S1 and table S1 (available online at stacks.iop.org/JMM/32/044003/mmedia) represent the roughness of the composite paper.

Figure 3(a) shows the digital photographs of M/BC$_x$ at different ratios. Figure 3(b) shows an airplane folded with the M/BC$_x$ composite paper as a conductor in a circuit to light LEDs, which vividly shows that the M/BC$_x$ composite paper has excellent thinness, durability and conductivity, and has the potential to be used as friction nanogenerator electrodes. The mass of the composite paper is 10 mg (figure 3(c)). XRD tests

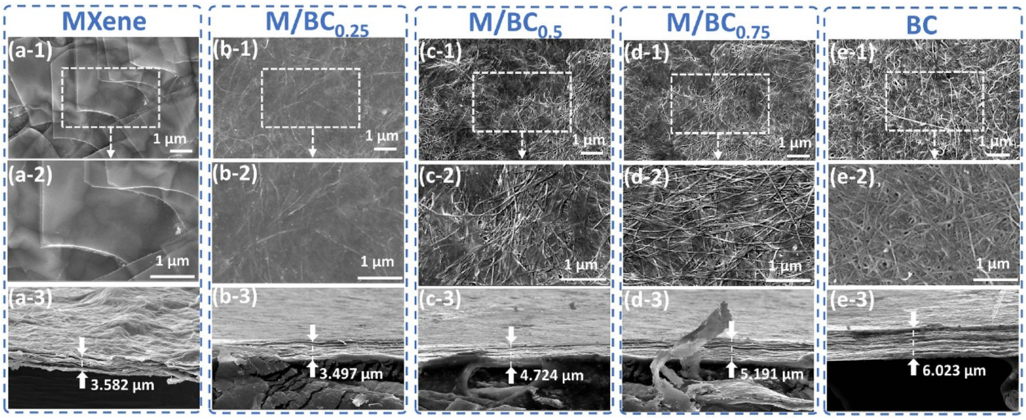

Figure 2. SEM images of the M/BC$_x$ composite paper. (a) MXene. (b) M/BC$_{0.25}$. (c) M/BC$_{0.5}$. (d) M/BC$_{0.75}$. (e) BC.

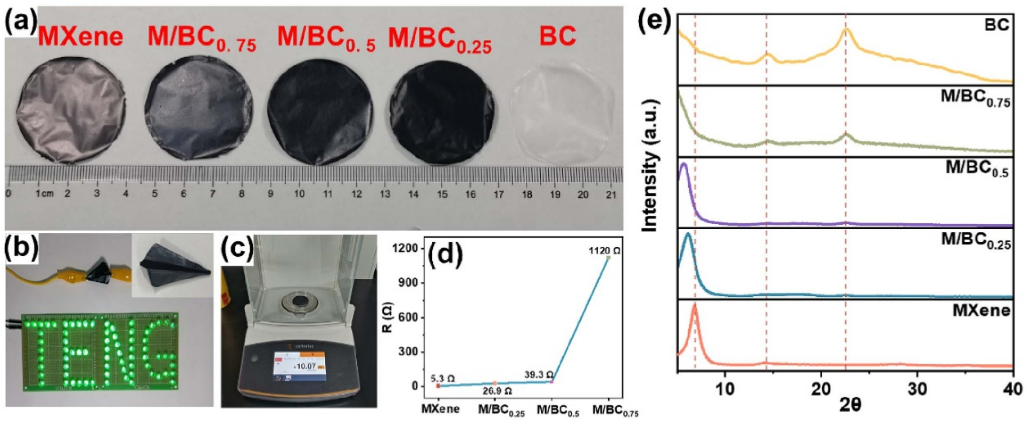

Figure 3. (a) Digital photos of the M/BC$_x$ composite paper. (b) M/BC$_{0.5}$ paper folded into an airplane and remains conductive in a circuit. (c) Weight of M/BC$_x$. (d) Resistance measurement of M/BC$_x$. (e) XRD pattern of M/BC$_x$.

are performed on the M/BC$_x$ composite paper (figure 3(e)), and the pure MXene paper show strong (002) diffraction peaks around 7°, and peaks at 14.1° and 22.7° are characteristic peaks of pure BC fibers. The (002) diffraction peak of MXene shifts to a lower 2θ angle as the BC content increases, which indicates that the lattice parameters of the M/BC$_x$ composite paper with 1D BC inserted become larger compared to the pure MXene paper. Meanwhile, with the increase of BC content, the two characteristic peaks corresponding to BC begin to increase.

3.2. Preparation process and working mechanism of M/BC$_x$-TENG

Figure 4(a) shows the preparation process of the nanogenerator. Figures 4(b) and (c) shows the microscopic morphology photos of PTFE and M/BC$_{0.5}$ composite paper. According to the frictional electron sequence, PTFE is frictionally electronegative and has a significant difference in its ability to attract and retain electrons compared to MXene/BC, which produce a large electrical output of TENG.

The operating mechanism of the vertical contact separation mode M/BC$_x$-TENG is shown in figure 4(d). When the Cu/PTFE plate gets in contact with the M/BC$_x$ plate driven by a force, electrons are transferred from the M/BC$_x$ electrode into the PTFE and create a positive charge on the M/BC$_x$ surface and a negative charge on the PTFE surface. When the external force is withdrawn, separation of the two surface is created by the spring and then a potential difference is created between these two films. The potential difference drives the electrons to flow from the Cu/PTFE electrode to the M/BC$_x$ electrode through an external circuit to counteract the positive frictional charge on the M/BC$_x$ plate. When an external force is applied again to bring the two electrodes into contact, the potential difference begins to decrease. As a result, I_{SC} drops from a maximum value to zero when the electrodes are in full contact with each other again. The reduction in spacing causes the PTFE plate to have a higher potential than the M/BC$_x$ plate. Therefore, electrons flow from the M/BC$_x$ electrode to the Cu/PTFE electrode through an external circuit to shield the positive charges on the PTFE plate.

3.3. M/BC$_x$-TENG electrical output performance characterization

To evaluate the electrical output performance of the M/BC$_x$-TENG, a mechanical linear motor is used to provide periodic contact separation motion. The maximum moving distance

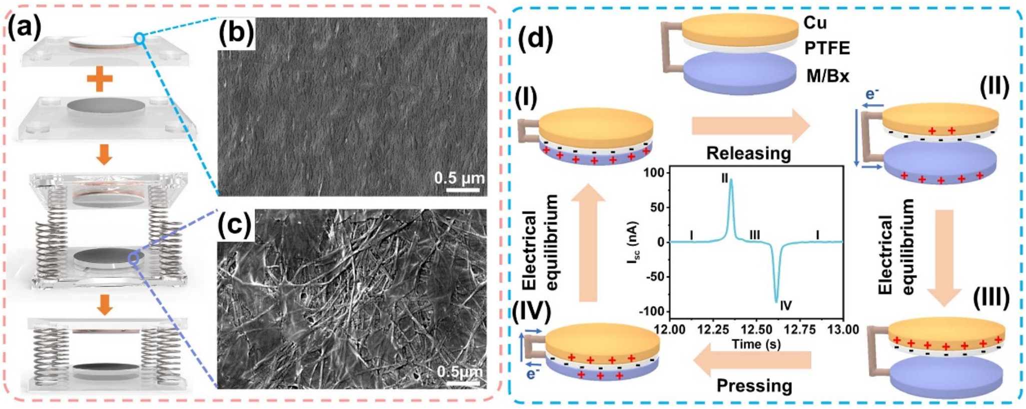

Figure 4. (a) Preparation process of TENG. (b), (c) SEM images of PTFE and M/$BC_{0.5}$. (d) Working mechanism of TENG: (I) external force brings the two electrodes into contact with each other, generating surface frictional charge; (II) withdrawal of force leads to separation and flow of electrons from the copper electrode to M/BC_x through an external circuit; (III) electrical equilibrium of TENG after charge distribution; (IV) external force is applied again, bringing the two electrodes into contact and causing electrons to flow from M/BC_x to the copper electrode via an external circuit.

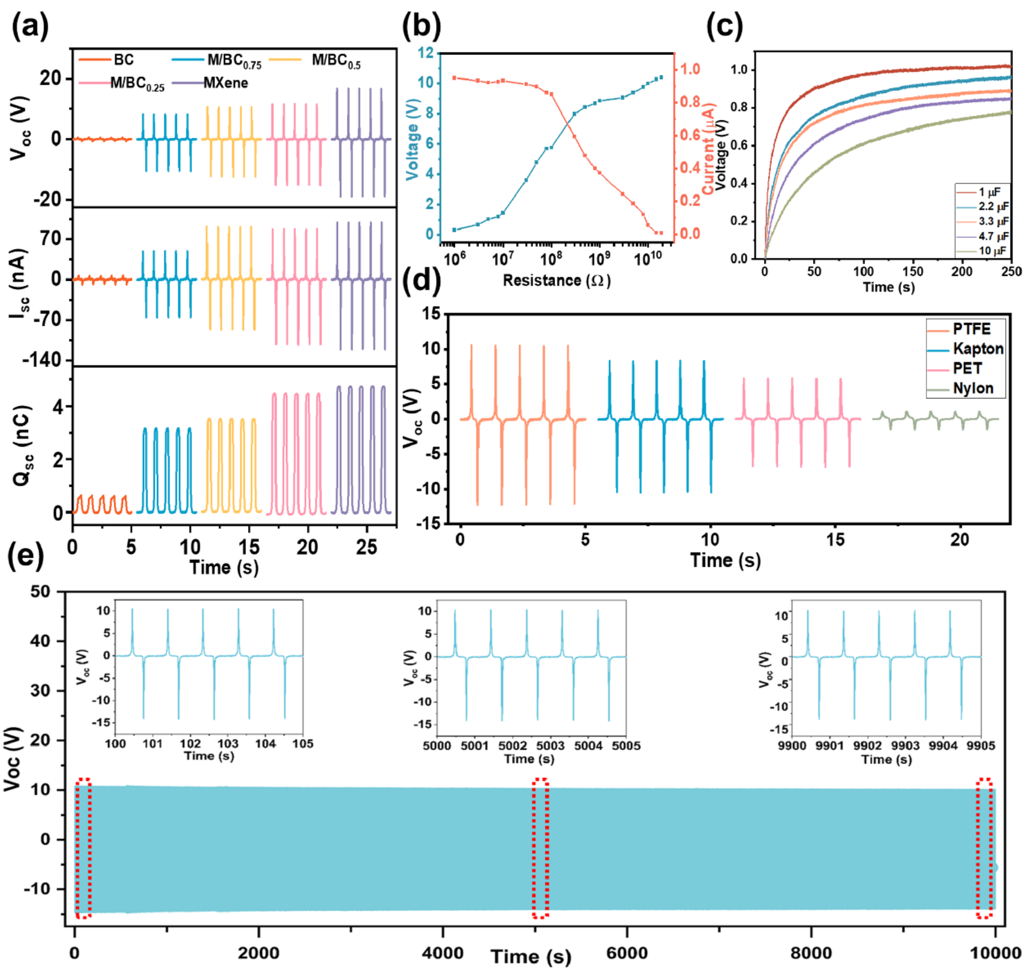

Figure 5. (a) Representation of V_{OC}, I_{SC}, and Q_{SC} for M/BC_x-TENG. (b) Output voltage and output current for M/$BC_{0.5}$ with different load resistances. (c) Different capacitance capacities (1–10 μF). (d) Output voltage for different materials with M/$BC_{0.5}$. (e) Test of the stability of the TENS for heavy metal ion detection.

is 20 mm and the operating frequency is 1 Hz. A video of the experiment trials is recorded as video S1 in the supplementary materials. In order to analyze the effect of BC mass ratio in M/BC_x composite paper on the output performance of M/BC_x-TENG, samples with different BC ratios are prepared. The output performance of both V_{OC}, I_{SC}, and Q_{SC}

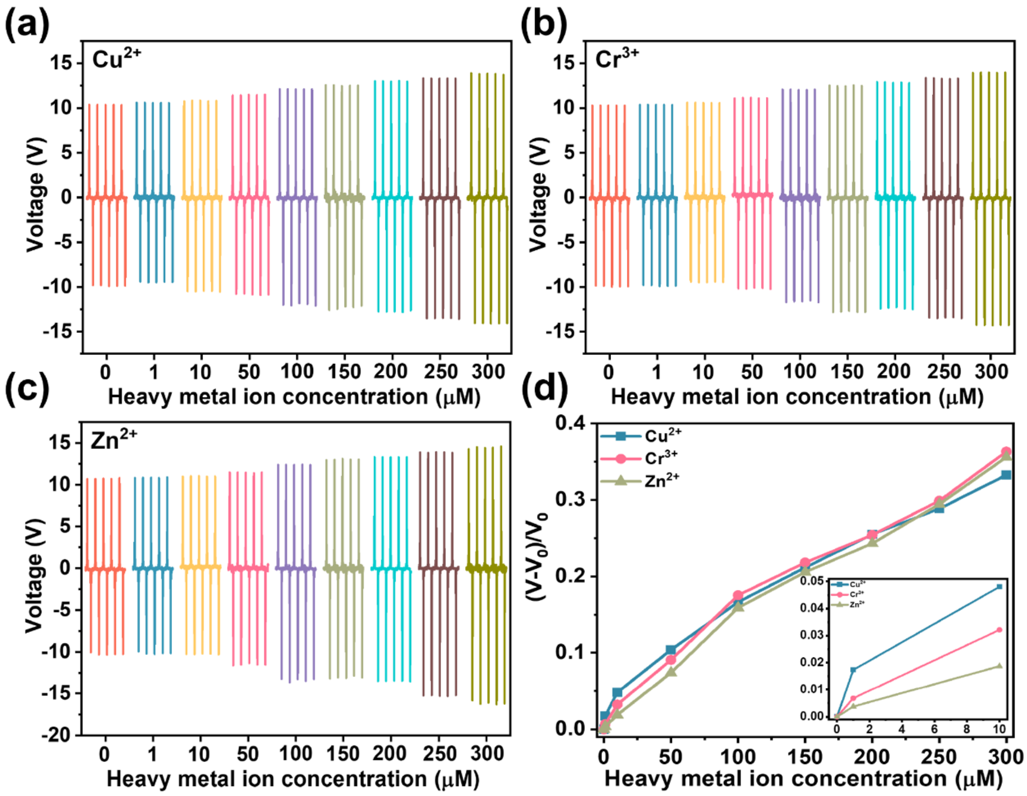

Figure 6. Characterization of the heavy metal ion detection performance of the M/$BC_{0.5}$-TENS. (a)–(c) Variation of V_{OC} with the Cu^{2+}, Cr^{3+}, and Zn^{2+} concentrations, respectively. (d) Sensitivity test of the developed TENS for the detection of Cu^{2+}, Cr^{3+}, Zn^{2+} ions.

decreases with increasing BC content (figure 5(a)). This can be attributed to the insulating properties of BC. As shown in figure 5(a), the V_{OC}, I_{SC}, and $Q_{SC\,c}$ of M/$BC_{0.5}$ are 10.9 V, 90 nA and 3.5 nC, respectively, much higher than those of M/$BC_{0.75}$, but not much lower than those of M/$BC_{0.25}$. To balance the electrical performance and the mechanical properties, as well as the fabrication cost of the composite paper, we choose M/$BC_{0.5}$ as the friction layer and electrode of TENG.

The output voltage and current at different external load resistances is measured, from 1 MΩ to 19 GΩ. The voltage increases with larger external load resistance, and the current shows a decreasing trend according to Ohm's law, as shown in figure 5(b). The charging capability of M/$BC_{0.5}$-TENG is also measured in a rectifier circuit with M/$BC_{0.5}$-TENG, bridge rectifier, and commercial capacitors. As shown in figure 5(c), the 1 μF capacitor is charged to 1 V in 100 s, and the 10 μF capacitor is charged to 0.7 V in 250 s.

In addition, we investigate the V_{OC} of M/$BC_{0.5}$ with different materials as the other friction layer. The output variation corresponds to the triboelectric series of the materials. The highest V_{OC} of 10.9 V is obtained with PTFE and the smallest V_{OC} is obtained with nylon. The stability of the TENS is further evaluated. After 10 000 cycles of continuous operation, no drop in V_{oc} is observed, as shown in figure 5(e), which can be attributed to the excellent mechanical properties of our M/$BC_{0.5}$ composite paper, indicating good stability of this TENS.

3.4. Characterization of M/$BC_{0.5}$-TENS for heavy metal ion detection

To verify the detection capability of the M/$BC_{0.5}$-TENG as sensor for heavy metal ions, three heavy metal ions commonly found in industrial wastewater, Zn^{2+}, Cu^{2+} and Cr^{3+} [32], are investigated. In the experiments, constant volumes of heavy metal ion solutions (20 μl) are dropped onto the surface of M/$BC_{0.5}$ composite paper. After drying at ambient temperature (24 °C), electrical measurements are performed. The V_{oc} varies with Cu^{2+} concentration as shown in figure 6(a). In the range of 1–300 μM, the V_{oc} is a monotonically increasing mode. MXene has a large specific surface area and abundant surface functional groups, which provide many sites for heavy metal ion adsorption. The adsorption of Cu^{2+} increases the tendency of the surface to gain electrons; therefore the V_{oc} increases sensitively with the addition of the metal ions on the MX/BC composite paper. Similarly, Cr^{3+} and Zn^{2+} open-circuit voltages show similar trends (figures 6(b) and (c)). The sensing performance of the TENS for the detection of heavy metal ions is evaluated by the ratio of V_{OC} ($(V - V_0)/V_0$), as shown in figure 6(d). The TENS makes good responses in electric signals to the ion concentration changes as low as 1 μM. This high sensitivity is most likely related to the unique physicochemical properties of MXene. The large number of defective sites on the surface of MXene, on which the metal ions are prone to be adsorbed, can change the electron gain/loss capacity greatly with very slight ion concentration disturbance. In a previous report, Li *et al* added coordination molecules for help and get a detection limit of 40 μM heavy metal ions using their TENS with Cu and PTFE as the friction layers [21]. Here we make use of the abundant defect sites on the surface of MXene and largely improve the sensitivity of TENS. The linearity of the TENS in the concentration range of 10–300 μM for Cu^{2+}, Cr^{2+}, Z^{n2+} are 0.98311, 0.97787, 0.98383, respectively (figure S2).

4. Conclusion

In this work, we fabricate a novel ultra-thin M/BC composite paper, based on which we develop a self-powered TENS based on the frictional electric effect for the detection of heavy metal ions. For the detection of Cu^{2+}, Cr^{3+}, Zn^{2+}, the TENS works well in the detection range of 1–300 μM and linear range of 10–300 μM, under the condition that no ligand molecules are required. This suggests that the TENS is capable of detecting the toxicity range of heavy metals as specified by WHO. To the best of our knowledge, this is the first try to combine MXene, bacteria cellulose and TENS to do ion sensing. This TENS has high sensitivity, good stability, and is based on a self-powered technology that can be widely applied in practice. This TENS has potential applications in industrial wastewater monitoring, as well as clinical toxicology monitoring.

Data availability statement

All data that support the findings of this study are included within the article (and any supplementary files).

Acknowledgments

This work is supported by the National Natural Science Foundation of China (81971770, T2125003, 61875015), and Beijing Municipal Natural Science Foundation (JQ20038).

ORCID iDs

Engui Wang https://orcid.org/0000-0002-8125-5659
Hongqing Feng https://orcid.org/0000-0003-2767-3080
Zhou Li https://orcid.org/0000-0002-9952-7296

References

[1] He Z L, Yang X E and Stoffella P J 2005 Trace elements in agroecosystems and impacts on the environment *J. Trace Elem. Med. Biol.* **19** 125–40
[2] Harindintwali J D, Zhou J and Yang W 2020 Biochar-bacteria-plant partnerships: eco-solutions for tackling heavy metal pollution *Ecotoxicol. Environ. Saf.* **204** 111020
[3] Askari M S, Alamdari P, Chahardoli S and Afshari A 2020 Quantification of heavy metal pollution for environmental assessment of soil condition *Environ. Monit. Assess.* **192** 162
[4] Yue L, Ma C, Du J, Li F and Zhang H 2020 Recent advance on biochar remediation of heavy metal pollution in soil *Fresenius Environ. Bull.* **29** 7166–70
[5] Bao P, Gao X-L and Wen G-Q 2020 The threat of antibiotics and heavy metal pollution to human health and potential solutions *Biomed. Res. Int.* **2020** 1–2
[6] Bansod B, Kumar T, Thakur R, Rana S and Singh I 2017 A review on various electrochemical techniques for heavy metal ions detection with different sensing platforms *Biosens. Bioelectron.* **94** 443–55
[7] Quang D T and Kim J S 2010 Fluoro-and chromogenic chemodosimeters for heavy metal ion detection in solution and biospecimens *Chem. Rev.* **110** 6280–301
[8] He Q, Miller E W and Wong A P 2006 A selective fluorescent sensor for detecting lead in living cells *J. Am. Chem. Soc.* **128** 9316–7
[9] Wang S, Forzani E S and Tao N 2007 Detection of heavy metal ions in water by high-resolution surface plasmon resonance spectroscopy combined with anodic stripping voltammetry *Anal. Chem.* **79** 4427–32
[10] Fan F-R, Tian Z-Q and Lin Wang Z 2012 Flexible triboelectric generator *Nano Energy* **1** 328–34
[11] Wu H, Li H and Wang X 2020 A high-stability triboelectric nanogenerator with mechanical transmission module and efficient power management system *J. Micromech. Microeng.* **30** 115017
[12] Feng H, Bai Y, Qiao L, Li Z, Wang E, Chao S, Qu X, Cao Y, Liu Z and Han X 2021 An ultra-simple charge supplementary strategy for high performance rotary triboelectric nanogenerators *Small* **17** 2101430
[13] Jiang D, Ouyang H, Shi B, Zou Y, Tan P, Qu X, Chao S, Xi Y, Zhao C and Fan Y 2020 A wearable noncontact free-rotating hybrid nanogenerator for self-powered electronics *InfoMat* **2** 1191–200
[14] Han J, Li H and Fu T 2021 A pulsed freestanding triboelectric nanogenerator and power management circuit to harvest rotation energy from an automobile brake *J. Micromech. Microeng.* **31** 015007
[15] Shi Q, Wang H, Wu H and Lee C 2017 Self-powered triboelectric nanogenerator buoy ball for applications ranging from environment monitoring to water wave energy farm *Nano Energy* **40** 203–13
[16] Zhu M, Yi Z, Yang B and Lee C 2021 Making use of nanoenergy from human—nanogenerator and self-powered sensor enabled sustainable wireless IoT sensory systems *Nano Today* **36** 101016
[17] Garcia C and Trendafilova I 2019 Triboelectric sensor as a dual system for impact monitoring and prediction of the damage in composite structures *Nano Energy* **60** 527–35
[18] Garcia C and Trendafilova I 2019 Real-time diagnosis of small energy impacts using a triboelectric nanosensor *Sens. Actuators* A **291** 196–203
[19] Garcia C, Trendafilova I and Sanchez del Rio J 2019 Detection and measurement of impacts in composite structures using a self-powered triboelectric sensor *Nano Energy* **56** 443–53
[20] Jie Y, Wang N, Cao X, Xu Y, Li T, Zhang X and Wang Z L 2015 Self-powered triboelectric nanosensor with poly (tetrafluoroethylene) nanoparticle arrays for dopamine detection *ACS Nano* **9** 8376–83
[21] Li Z, Chen J, Guo H, Fan X, Wen Z, Yeh M H, Yu C, Cao X and Wang Z L 2016 Triboelectrification-enabled self-powered detection and removal of heavy metal ions in wastewater *Adv. Mater.* **28** 2983–91
[22] Lin Z-H, Xie Y, Yang Y, Wang S, Zhu G and Wang Z L 2013 Enhanced triboelectric nanogenerators and triboelectric nanosensor using chemically modified TiO_2 nanomaterials *ACS Nano* **7** 4554–60
[23] Lin Z H, Zhu G, Zhou Y S, Yang Y, Bai P, Chen J and Wang Z L 2013 A self-powered triboelectric nanosensor for mercury ion detection *Angew. Chem., Int. Ed. Engl.* **52** 5065–9

[24] Zhou Q, Pan J, Deng S, Xia F and Kim T 2021 Triboelectric nanogenerator-based sensor systems for chemical or biological detection *Adv. Mater.* **33** 2008276
[25] Anichini C, Czepa W, Pakulski D, Aliprandi A and Ciesielski A 2018 Chemical sensing with 2D materials *Chem. Soc. Rev.* **47** 4860–908
[26] Zhang H 2018 Introduction: 2D materials chemistry *J. Chem. Rev.* **118** 6089–90
[27] Chen M, Liu D, Du X, Lo K H, Wang S, Zhou B and Pan H 2020 2D materials: excellent substrates for surface-enhanced Raman scattering (SERS) in chemical sensing and biosensing *TRAC Trends Anal. Chem.* **130** 115983
[28] Jingyuan C, Jing L, Shaokang R, Shao S and Lianhui W 2019 Construction and application of DNA-two-dimensional layered nanomaterials sensing platform *Acta Chim. Sin.* **77** 1230–8
[29] Su S, Sun Q, Gu X, Xu Y, Shen J, Zhu D, Chao J, Fan C and Wang L 2019 Two-dimensional nanomaterials for biosensing applications *TRAC Trends Anal. Chem.* **119** 115610
[30] Sharma S, Chhetry A, Sharifuzzaman M, Yoon H and Park J Y 2020 Wearable capacitive pressure sensor based on MXene composite nanofibrous scaffolds for reliable human physiological signal acquisition *ACS Appl. Mater.* **12** 22212–24
[31] Mao L, Hu S, Gao Y, Wang L, Zhao W, Fu L, Cheng H, Xia L, Xie S and Ye W 2020 Biodegradable and electroactive regenerated bacterial cellulose/MXene ($Ti_3C_2T_x$) composite hydrogel as wound dressing for accelerating skin wound healing under electrical stimulation *Adv. Healthcare Mater.* **9** 2000872
[32] Jiao S, Zhou A, Wu M and Hu H 2019 Kirigami patterning of MXene/bacterial cellulose composite paper for all-solid-state stretchable micro-supercapacitor arrays *Adv. Sci.* **6** 1900529
[33] Chen Z, Hu Y, Zhuo H, Liu L, Jing S, Zhong L, Peng X and Sun R-C 2019 Compressible, elastic, and pressure-sensitive carbon aerogels derived from 2D titanium carbide nanosheets and bacterial cellulose for wearable sensors *Chem. Mater.* **31** 3301–12
[34] Cui Z, Gao C, Fan Z, Wang J, Cheng Z, Xie Z, Liu Y and Wang Y 2021 Lightweight MXene/cellulose nanofiber composite film for electromagnetic interference shielding *J. Electron. Mater.* **50** 2101–10
[35] Gumpu M B, Sethuraman S, Krishnan U M and Rayappan J B B 2015 A review on detection of heavy metal ions in water—an electrochemical approach *Sens. Actuators* B **213** 515–33
[36] Naguib M, Kurtoglu M, Presser V, Lu J, Niu J, Heon M, Hultman L, Gogotsi Y and Barsoum M W 2011 Two-dimensional nanocrystals produced by exfoliation of Ti_3AlC_2 *Adv. Mater.* **23** 4248–53